DOI: 10.1002/chem.201101923

Dye-Sensitized Solar Cells Based on Donor-π-Acceptor Fluorescent Dyes with a Pyridine Ring as an Electron-Withdrawing-Injecting Anchoring Group

Yousuke Ooyama, Tomoya Nagano, Shogo Inoue, Ichiro Imae, Kenji Komaguchi, Joji Ohshita, and Yutaka Harima*[a]

Abstract: A new-type of donor–acceptor π-conjugated (D-π-A) fluorescent dyes **NI3**–**NI8** with a pyridine ring as electron-withdrawing-injecting anchoring group have been developed and their photovoltaic performances in dye-sensitized solar cells (DSSCs) are investigated. The short-circuit photocurrent densities and solar energy-to-electricity conversion yields of DSSCs based on **NI3**–**NI8** are greater than those for the conventional D-π-A dye sensitizers **NI1** and **NI2** with a carboxyl group as the electron-withdrawing anchoring group. The IR spectra of **NI3**–**NI8** adsorbed on TiO_2 indicate the formation of coordinate bonds between the pyridine ring of dyes **NI3**–**NI8** and the Lewis acid sites (exposed Ti^{n+} cations) of the TiO_2 surface. This work demonstrates that the pyridine rings of D-π-A dye sensitizers that form a coordinate bond with the Lewis acid site of a TiO_2 surface are promising candidates as not only electron-withdrawing anchoring group but also electron-injecting group, rather than the carboxyl groups of the conventional D-π-A dye sensitizers that form an ester linkage with the Brønsted acid sites of the TiO_2 surface.

Keywords: donor–acceptor systems · dyes/pigments · fluorescence · sensitizers · solar cells

Introduction

During the last two decades, dye-sensitized solar cells (DSSCs) have received considerable attention because of their high incident solar light-to-electricity conversion efficiency and low cost of production.[1–11] To increase the power conversion efficiency, much research has focused on the development of new dye sensitizers and electrolytes and the improvement of nanocrystalline TiO_2 electrodes. In particular, as the most promising organic dye sensitizers for DSSCs, many kinds of donor–acceptor π-conjugated (D-π-A) dyes with both electron-donating (D) and electron-accepting (A) groups linked by a π-conjugated bridge, which exhibit broad and intense absorption, have been developed.[2–11] The spectral features of the D-π-A dyes are associated with the intramolecular charge transfer (ICT) excitation from the donor to acceptor moiety of the dye, which leads to efficient electron transfer from the excited dye through the acceptor moiety into the conduction band (CB) of TiO_2. Most of the D-π-A dyes, such as coumarin, polyene, thiophene, and indoline dyes, for DSSCs developed so far have a dialkyl amine or diphenylamine moiety as electron donor, and a carboxylic acid, cyanoacrylic acid, or rhodanine-3-acetic acid moiety that acts as electron acceptor as well as anchoring group for attachment on a TiO_2 surface. The carboxyl group enables good electron communication between the dye and TiO_2 by forming a strong ester linkage with Brønsted acid sites (surface-bound hydroxyl groups) of the TiO_2 surface. Recently, as a successful molecular design of D-π-A dyes to improve the performances of DSSCs, a new series of donor–acceptor substituted squaraine dyes and porphyrin dyes providing good absorption in the red/near-IR region of the solar spectrum have been designed and developed.[12,13] DSSCs based on the D-π-A dyes have reached power conversion efficiencies as high as 10–11%, comparable to those of Ru complexes. However, the fact is that the photovoltaic performances of DSSCs based on D-π-A dyes have tended to stagnate for the last few years. To achieve a breakthrough in the development of new and efficient D-π-A dyes for DSSCs, an epoch-making molecular design, such as formation of a strong interaction between the electron-accepting moiety of sensitizers and the TiO_2 surface, is required.

On the other hand, very recently, as a new-type of D-π-A dye sensitizers for DSSCs, we have designed and synthesized fluorescent dyes **NI3**–**NI6** with a pyridine ring as electron-withdrawing anchoring group (Scheme 1).[14] The FTIR spectra of **NI3**–**NI6** adsorbed on TiO_2 nanoparticles indicate strong coordinate bonding between the pyridine ring of the dyes and the Lewis acid sites of the TiO_2 surface. The short-circuit photocurrent densities (J_{sc}) and solar energy-to-electricity conversion yields (η) of DSSCs based on **NI3**–**NI6** are greater than those of the conventional D-π-A dye sensitizers **NI1** and **NI2** with a carboxyl group as the electron-with-

[a] Dr. Y. Ooyama, T. Nagano, S. Inoue, Dr. I. Imae, Dr. K. Komaguchi, Prof. Dr. J. Ohshita, Prof. Dr. Y. Harima
Department of Applied Chemistry
Graduate School of Engineering
Hiroshima University
Higashi-Hiroshima 739-8527 (Japan)
Fax: (+81) 82-424-5494
E-mail: harima@mls.ias.hiroshima-u.ac.jp

Supporting information for this article is available on the WWW under http://dx.doi.org/10.1002/chem.201101923.

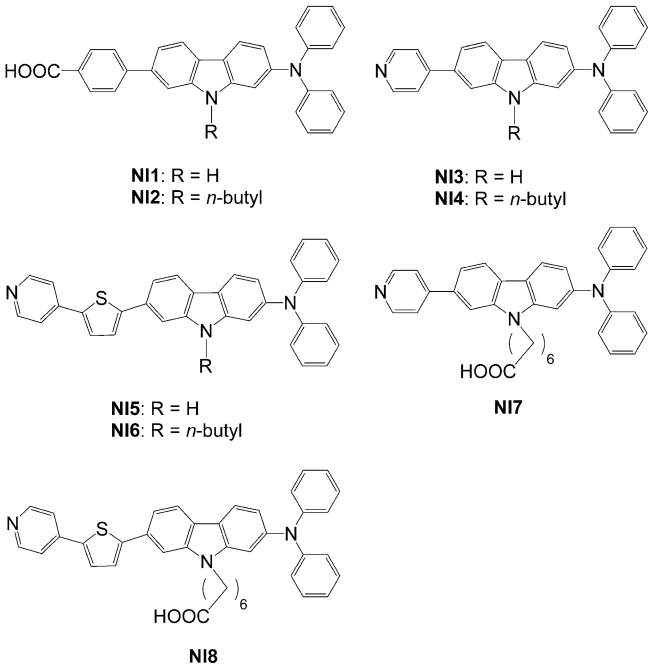

Scheme 1. Chemical structures of D-π-A fluorescent dyes **NI1**–**NI8**.

drawing anchoring group. Consequently, it was demonstrated that the formation of coordinate bonds between the pyridine ring of dyes **NI3**–**NI6** and the Lewis acid sites of the TiO_2 surface leads to efficient electron injection owing to the good electron communication between them, rather than the formation of an ester linkage between dyes **NI1** and **NI2** and the Brønsted acid sites of the TiO_2 surface.

In this work, to ensure the usefulness of the pyridine ring as an efficient electron-injecting group of new-type D-π-A dye sensitizers in DSSCs, we have designed and synthesized D-π-A fluorescent dyes **NI7** and **NI8** with a pyridine ring as electron-accepting group and carboxyl group as anchoring group. Dyes **NI7** and **NI8** have a nonconjugated alkyl chain containing a carboxyl group at the end position, so that the carboxyl group as an anchoring group is separated from the electron-acceptor moiety (Scheme 1; detailed synthetic procedures for the dyes are given in the Supporting Information). The IR spectra of **NI7** and **NI8** adsorbed on TiO_2 nanoparticles indicate the formation of coordinate bonds between the pyridine ring of dyes **NI7** and **NI8** and the Lewis acid sites of the TiO_2 surface. Herein, we report the photovoltaic performances of DSSCs based on new-type D-π-A fluorescent dyes **NI3**–**NI8** and propose the use of a pyridine ring as not only electron-withdrawing anchoring group but also electron-injecting group in place of the carboxyl group in conventional D-π-A dye sensitizers.

Results and Discussion

Spectroscopic properties of NI1–NI8 in solution and adsorbed on TiO_2 nanoparticles: The absorption and fluorescence spectra of **NI1**–**NI8** in 1,4-dioxane are shown in Figure 1 and the spectral data are summarized in Table 1. All the dyes show two absorption maxima: one band appears at around 300–315 nm ascribed to a π→π* transition, and the other band occurs at around 370–400 nm assigned to the ICT excitation from D (diphenylamino group) to A (carboxyphenyl group for **NI** and **NI2** and pyridine ring for **NI3**–**NI8**). The ICT bands of **NI5**, **NI6**, and **NI8** occur at a longer wavelength by approximately 20 nm than those of **NI1**–**NI4** and **NI7**. Furthermore, the molar extinction coefficients (ε) for the ICT bands of **NI5**, **NI6**, and **NI8** are around $50\,000\,M^{-1}cm^{-1}$, higher than the $30\,000$–$35\,000\,M^{-1}cm^{-1}$ for **NI1**–**NI4** and **NI7**. These results show that the introduction of a thiophene unit on the carbazole

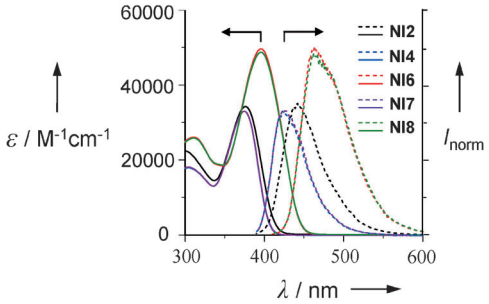

Figure 1. Absorption (·····) and fluorescence (——) spectra of **NI2**, **NI4**, and **NI6**–**NI8** in 1,4-dioxane. I_{norm} = normalized fluorescence intensity.

Table 1. Optical and electrochemical data, HOMO and LUMO energy levels, and DSSC performance parameters of **NI1**–**NI8**.

Dye	λ_{abs} [nm] (ε [$M^{-1}cm^{-1}$])[a]	λ_{em} [nm] (Φ_f)[b]	$E^{ox}_{1/2}$ [V][c]	HOMO [V][d]	LUMO [V][d]	Molecules [cm^{-2}][e]	J_{sc} [$mA\,cm^{-2}$][f]	V_{oc} [mV][f]	FF[f]	η [%][f]
NI1	374 (34900)	438 (0.89)	0.30	0.93	−2.12	5.3×10^{16}	1.99	516	0.59	0.60
						10.4×10^{16}	2.96	503	0.61	0.91
NI2	376 (34300)	442 (0.87)	0.37	1.00	−2.03	4.8×10^{16}	1.80	517	0.60	0.56
						10.8×10^{16}	3.07	520	0.61	0.97
NI3	372 (30200)	423 (0.83)	0.34	0.97	−2.15	4.9×10^{16}	3.16	524	0.63	1.04
NI4	375 (33000)	423 (0.84)	0.39	1.02	−2.07	4.7×10^{16}	3.35	522	0.62	1.15
NI5	394 (48100)	465 (0.60)	0.30	0.93	−1.93	7.9×10^{16}	5.80	540	0.60	1.89
NI6	396 (49600)	464 (0.58)	0.34	0.97	−1.87	8.0×10^{16}	5.63	548	0.60	1.84
NI7	375 (33000)	425 (0.85)	0.38	1.01	−2.08	11.7×10^{16}	5.16	568	0.62	1.81
NI8	396 (48700)	467 (0.58)	0.34	0.97	−1.87	11.4×10^{16}	7.04	568	0.59	2.35

[a] In 1,4-dioxane. [b] In 1,4-dioxane. Fluorescence quantum yields (Φ_f) were determined by using a calibrated integrating sphere system (λ_{ex} = 370 nm). [c] Half-wave potentials for oxidation ($E^{ox}_{1/2}$) versus ferrocene/ferrocenium (Fc/Fc^+) were recorded in CH_2Cl_2/Bu_4NClO_4 (0.1 M) solution. [d] Versus the normal hydrogen electrode (NHE). [e] The adsorption amount per unit area of TiO_2 film was controlled by the immersion time of the TiO_2 electrode in the dye solution. [f] The photocurrent–voltage characteristics were measured under simulated solar light (air mass (AM) 1.5, 100 $mW\,cm^{-2}$). FF = fill factor.

skeleton expands the π conjugation in the dye and thus results in a redshift of the absorption maximum and enhancement of ε. The corresponding fluorescence maximum (λ_{em}) occurs at around 420–470 nm. The fluorescent dyes **NI1**–**NI4** and **NI7** (Φ_f = ca. 0.85) exhibit a higher fluorescence quantum yield than **NI5**, **NI6**, and **NI8** (Φ_f = ca. 0.6).

The absorption spectra of the dyes adsorbed on TiO_2 nanoparticles are shown in Figure 2. The absorption peak

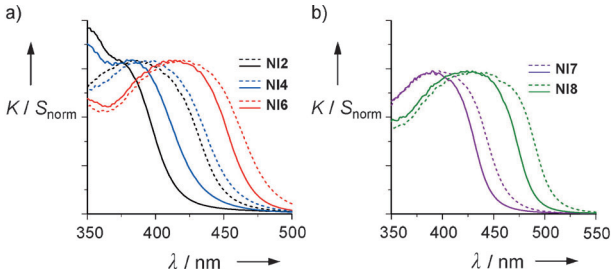

Figure 2. Absorption spectra of a) **NI2**, **NI4**, and **NI6** and b) **NI7** and **NI8** adsorbed on TiO_2 nanoparticles with (——) and without (•••••) CDCA as coadsorbent. The *y* axis is expressed in terms of the Kubelka–Munk equation $K/S=(1-R)^2/2R$, in which K is the absorption coefficient, S is the scattering coefficient, and R is the fractional reflectance.

wavelengths (λ_{abs}) are redshifted by about 10 nm for **NI1** and **NI2**, about 25 nm for **NI3**, **NI4**, and **NI7**, about 30 nm for **NI5** and **NI6**, and about 40 nm for **NI8** compared with those in 1,4-dioxane. Chenodeoxycholic acid (CDCA) was employed as coadsorbent to prevent dye aggregation on the TiO_2 surface. When CDCA is coadsorbed with **NI3**–**NI8** on TiO_2, the absorption peak wavelengths are blueshifted by about 10 nm for **NI3**, **NI4**, and **NI7**, about 20 nm for **NI5** and **NI6**, and about 10 nm for **NI8**, although the peak wavelengths are still redshifted compared with those in 1,4-dioxane. In contrast, the absorption peak wavelengths of **NI1** and **NI2** adsorbed on TiO_2 with coadsorption of CDCA are similar to those in 1,4-dioxane. These results show that the redshifts of **NI3**–**NI8** by adsorption on TiO_2 are due to the strong interaction between the dyes and the TiO_2 surface, which will be discussed later along with the FTIR spectra of the dyes adsorbed on TiO_2.

Electrochemical properties of NI1–NI8 and their HOMO and LUMO energy levels: The electrochemical properties of all the dyes were determined by cyclic voltammetry (CV) in CH_2Cl_2 containing 0.1 M tetrabutylammonium perchlorate (Bu_4NClO_4). The potentials were referred to ferrocene/ferrocenium (Fc/Fc^+) as the internal reference. A typical CV curve of **NI8** is shown in Figure 3. The electrochemical properties of **NI1**–**NI8** are summarized in Table 1. The oxidation peaks of **NI1**–**NI8** were observed at 0.34–0.42 V versus Fc/Fc^+ and the corresponding reduction peaks appeared at 0.26–0.35 V, thus showing that the oxidized states of all the dyes are stable. The HOMO and LUMO energy levels of all the dyes were evaluated from the spectral analyses and the half-wave potentials for oxidation of **NI1**–**NI8** ($E^{ox}_{1/2}$ = 0.30–0.39 V). The HOMO energy levels for **NI1**–**NI8** were 0.93–

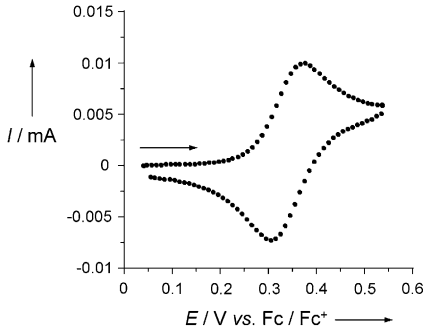

Figure 3. Cyclic voltammogram of **NI8** in CH_2Cl_2 containing Bu_4NClO_4 (0.1 M) at a scan rate of 50 mV s^{-1}. The arrow denotes the direction of the potential scan.

1.02 V with respect to a normal hydrogen electrode (NHE), which indicated that all the dyes have similar HOMO energy levels that are more positive than the I_3^-/I^- redox potential (0.4 V). This assures an efficient regeneration of the oxidized dyes by electron transfer from I^- in the electrolyte. The LUMO energy levels of the dyes were estimated from $E^{ox}_{1/2}$ and an intersection of absorption and fluorescence spectra (407 and 409 nm (3.05 and 3.03 eV) for **NI1** and **NI2**, respectively, 398, 401, and 401 nm (3.12, 3.09, and 3.09 eV) for **NI3**, **NI4**, and **NI7**, respectively, and 434, 436, and 436 nm (2.86, 2.84, and 2.84 eV) for **NI5**, **NI6**, and **NI8**, respectively). The LUMO energy levels of **NI1**–**NI8** were −2.12, −2.03, −2.15, −2.07, −1.93, −1.87, −2.08, and −1.87 V, respectively. The LUMO levels of **NI5**, **NI6**, and **NI8** are lower than those of **NI1**–**NI4** and **NI7**, which lead to the decrease of the energy gap between the HOMO and LUMO responsible for the redshift of ICT absorption bands for **NI5**, **NI6**, and **NI8** relative to **NI1**–**NI4** and **NI7**. Evidently, the LUMO energy levels of all the dyes are higher than the energy level of the CB of TiO_2 (−0.5 V), so that these dyes can efficiently inject electrons into the TiO_2 electrode.

Semiempirical MO calculations (AM1, INDO/S) of NI1–NI8: The photophysical properties of **NI1**–**NI8** were analyzed by using semiempirical molecular orbital (MO) calculations. The molecular structures were optimized by using the MOPAC/AM1 method,[15] and then the INDO/S method[16] was used for spectroscopic calculations. The calculated absorption wavelengths and the transition characters of the absorption bands are collected in Table 2. These calculated values for **NI1**–**NI8** are comparable to the observed spectra in 1,4-dioxane. The calculations indicate that the longest excitation bands were mainly assigned to the transition from HOMO to LUMO, for which HOMOs were mostly localized on the diphenylaminocarbazole moiety for **NI1**–**NI4** and **NI7** and the diphenylaminothiophenylcarbazole moiety for **NI5**, **NI6**, and **NI8**, and LUMOs were mostly localized on the carboxyphenylcarbazole moiety for **NI1** and **NI2**, the pyridinylcarbazole moiety for **NI3**, **NI4**, and **NI7**, and the pyridinylthiophenylcarbazole moiety for **NI5**, **NI6**, and **NI8**. The HOMO and LUMO of **NI2**, **NI4**,

Table 2. Calculated absorption spectral data for **NI1**–**NI8**.

Compound	Absorption (calcd) λ_{max} [nm]	f[a]	CI component[b]
NI1	348	1.13	HOMO→LUMO (41%)
NI2	348	1.08	HOMO→LUMO (40%)
NI3	345	0.96	HOMO→LUMO (65%)
NI4	345	0.87	HOMO→LUMO (61%)
NI5	378	1.84	HOMO→LUMO (65%)
NI6	378	1.83	HOMO→LUMO (65%)
NI7	344	0.84	HOMO→LUMO (59%)
NI8	377	1.84	HOMO→LUMO (65%)

[a] Oscillator strength. [b] The transition is shown by an arrow from one orbital to another, followed by its percentage configuration interaction (CI) component.

and **NI6**–**NI8** are shown in Figure 4a and b. The changes in the calculated electron density accompanied by the first electron excitation for **NI2**, **NI4**, and **NI6**–**NI8** are shown in Figure 4c, which reveal a strong ICT nature from the diphenylamino moiety to the carboxyphenyl group or pyridine ring upon illumination by light.

FTIR spectra of NI1–NI8 adsorbed on TiO_2 nanoparticles: To elucidate the adsorption states of dyes **NI1**–**NI8** on TiO_2 nanoparticles, we measured the FTIR spectra of the dye powders and the dyes adsorbed on TiO_2 nanoparticles. The examples of **NI2**, **NI4**, and **NI6**–**NI8** are shown in Figure 5. For the powders of dyes **NI1**, **NI2**, **NI7**, and **NI8**, the C=O stretching band of the carboxyl group was observed at 1680 cm^{-1}. When the dyes were adsorbed on the TiO_2 surface, the C=O stretching band at 1680 cm^{-1} disappeared. These observations indicate that the carboxyl groups of the dyes form an ester linkage with the TiO_2 surface.[17] On the other hand, the characteristic stretching bands for C=N or C=C were clearly observed at around 1590, 1490, and 1460 cm^{-1} for all the dye powders. In the FTIR spectra of

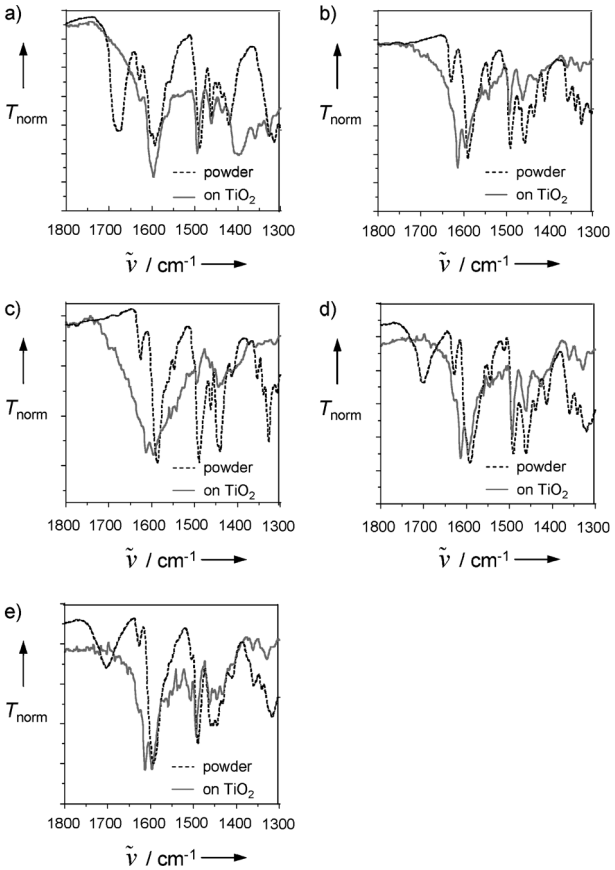

Figure 5. FTIR spectra of the dye powders and dyes adsorbed on TiO_2 nanoparticles for a) **NI2**, b) **NI4**, c) **NI6**, d) **NI7**, and e) **NI8**.

NI3–**NI8** adsorbed on TiO_2, a new band appeared at around 1615 cm^{-1}, which can be assigned to a pyridine ring coordinated to the Lewis acid sites of the TiO_2 surface.[18,19] This indicates that the dyes **NI1** and **NI2** are adsorbed on the TiO_2 surface by the ester linkage alone at Brønsted acid sites (surface-bound hydroxyl groups), whereas the dyes **NI3**–**NI6** are predominantly adsorbed on the TiO_2 surface by coordinate bonding at Lewis acid sites (exposed Ti^{n+} cations), and the dyes **NI7** and **NI8** are adsorbed on the TiO_2 surface by both the ester linkage and coordinate bonding. The strong coordinate bonding is responsible for the large red-shift of the absorption peak for **NI3**–**NI8** adsorbed on TiO_2 (Figure 2).

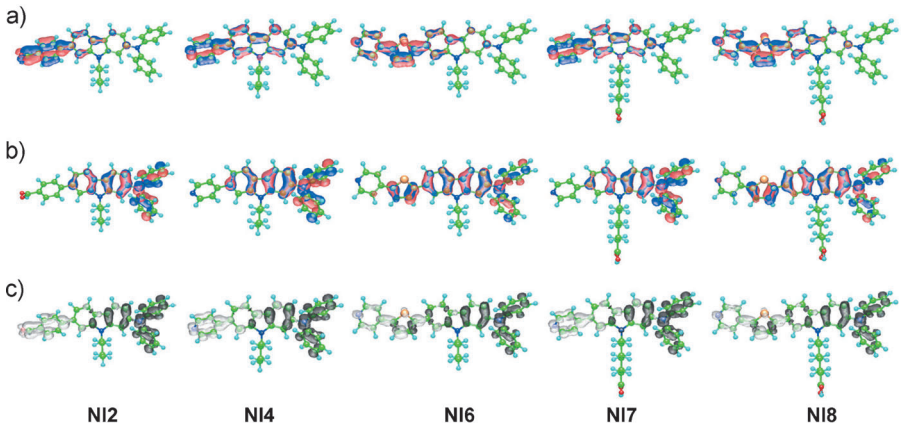

Figure 4. a) LUMO and b) HOMO of **NI2**, **NI4**, and **NI6**–**NI8**. The red and blue lobes denote the positive and negative phases, respectively, of the coefficients of the MOs. The size of each lobe is proportional to the MO coefficient. c) Calculated electron density changes accompanying the first electronic excitation of **NI2**, **NI4**, and **NI6**–**NI8**. The black and white lobes signify the decrease and increase in electron density accompanying the electronic transition, respectively. Their areas indicate the magnitude of the electron density change. (Light blue, green, blue, red, and gold balls correspond to hydrogen, carbon, nitrogen, oxygen, and sulfur atoms, respectively.)

Photovoltaic performances of DSSCs based on NI1–NI8: The

DSSCs were prepared by using the dye-adsorbed TiO_2 electrode, Pt-coated glass as a counter electrode, and an acetonitrile solution with iodine (0.05 M), lithium iodide (0.1 M), and 1,2-dimethyl-3-propylimidazolium iodide (0.6 M) as electrolyte. The photocurrent–voltage (*I–V*) characteristics were measured under simulated solar light (AM 1.5, 100 mW cm^{-2}). The *I–V* curves and the incident photon-to-current conversion efficiency (IPCE) spectra are shown in Figure 6. The photovoltaic performance parameters of

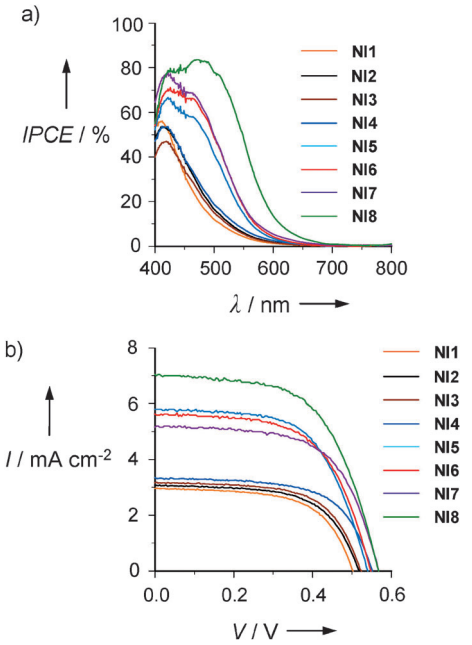

Figure 6. a) IPCE spectra and b) *I–V* curves of DSSCs based on **NI1**–**NI8**. The amounts of adsorbed dyes on TiO_2 film are 10.4×10^{16}, 10.8×10^{16}, 4.9×10^{16}, 4.7×10^{16}, 7.9×10^{16}, 8.0×10^{16}, 11.7×10^{16}, and 11.4×10^{16} molecules cm^{-2} for **NI1**–**NI8**, respectively. TiO_2 electrodes of thickness 9 μm were used. CDCA was not employed.

DSSCs based on the dyes **NI1**–**NI8** are collected in Table 1. The short-circuit photocurrent density (J_{sc}) and solar energy-to-electricity conversion yield (η) increase in the order **NI1** (2.96 mA cm^{-2}, 0.91 %) < **NI2** (3.07 mA cm^{-2}, 0.97 %) < **NI3** (3.16 mA cm^{-2}, 1.04 %) < **NI4** (3.35 mA cm^{-2}, 1.15 %) < **NI7** (5.16 mA cm^{-2}, 1.81 %), when comparisons are made of the maximum adsorption amounts of dyes adsorbed on TiO_2 (10.4×10^{16}, 10.8×10^{16}, 4.9×10^{16}, 4.7×10^{16}, and 11.7×10^{16} molecules cm^{-2} for **NI1**–**NI4** and **NI7**, respectively) under the adsorption condition of 1×10^{-4} M dye solution in THF. The open-circuit photovoltages (V_{oc}) for **NI1**–**NI4** and **NI7** are 503, 520, 524, 552, and 568 mV, respectively, which were slightly different among the five dyes. The maximum IPCE values of **NI1**–**NI4** (47–55 %) resemble each other very well. On the other hand, the maximum IPCE value (ca. 80 %) of **NI7** is higher than those of **NI1**–**NI4**.

To see explicitly the probability of electron injection from the dye to the CB of TiO_2, the adsorption amounts of dyes adsorbed on TiO_2 are plotted against the J_{sc} value for **NI1**–**NI4** and **NI7** in Figure 7. The J_{sc} values increase almost linearly with the increase in the adsorption amounts of dyes, although a salient feature to be noted in Figure 7 is the difference of the slope values: the slopes became steep in the

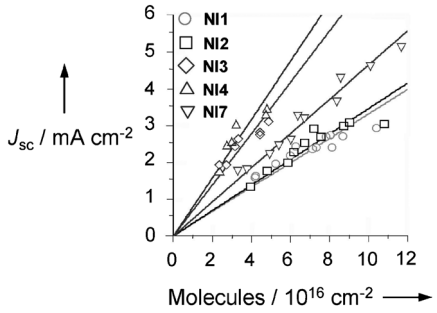

Figure 7. Plots of J_{sc} values against amounts of dye adsorbed on TiO_2 for **NI1**–**NI4** and **NI7**.

order **NI1** = **NI2** < **NI7** < **NI3** = **NI4**. As shown in Figure 8, this result indicates that the formation of strong coordinate bonds between the pyridine ring of dyes **NI3** and **NI4** and

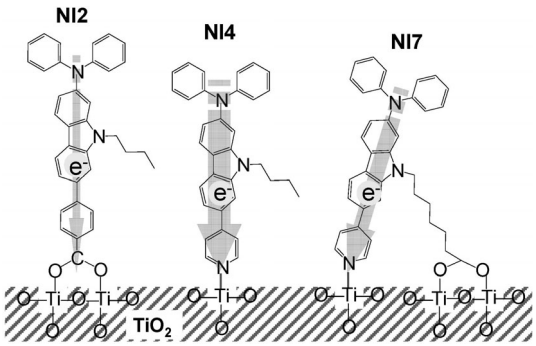

Figure 8. Configurations of **NI2**, **NI4**, and **NI7** on the TiO_2 surface.

the Lewis acid sites of the TiO_2 surface leads to an efficient electron injection owing to good electron communication between them, rather than the formation of an ester linkage between the dyes **NI1** and **NI2** and the Brønsted acid sites of the TiO_2 surface. On the other hand, the slope for **NI7** is smaller than those for **NI3** and **NI4**. It is reasonable to presume that the relatively less efficient electron injection for **NI7** is ascribable to weaker coordinate bonding between the pyridine ring of **NI7** and the Lewis acid sites of the TiO_2 surface because of the flexibility of the alkyl chain. Thus, our results demonstrate that the dyes **NI3**, **NI4**, and **NI7** can inject electrons efficiently from the pyridine ring as electron-withdrawing anchoring group to the CB of the TiO_2 electrode through strong coordinate bonding with the Lewis acid site of the TiO_2 surface. However, the maximum adsorption amounts of dyes adsorbed on TiO_2 for **NI3** and **NI4** are smaller than those for **NI1**, **NI2**, and **NI7**, because for the TiO_2 nanoparticles commonly used in DSSCs, the Lewis acid sites on the TiO_2 surface are fewer than the Brønsted

acid sites. Thus, further studies on the development of TiO_2 nanoparticles having Lewis acid sites enriched by treatment of the TiO_2 surface or hydrolysis of $TiCl_4$ with ammonium hydroxide are now in progress, to increase the adsorption amounts of the D-π-A dye sensitizers with pyridine rings as electron-withdrawing anchoring groups on TiO_2.

On the other hand, the J_{sc} and η values for **NI5** (5.80 mA cm^{-2}, 1.89%), **NI6** (5.63 mA cm^{-2}, 1.84%), and **NI8** (7.04 mA cm^{-2}, 2.35%) are larger than those for **NI3**, **NI4**, and **NI7**. The maximum IPCE values were 65–70% in the range from 410 to 470 nm for **NI5** and **NI6** and about 80% in the range from 420 to 500 nm for **NI8**. The relatively high photovoltaic performances of **NI5**, **NI6**, and **NI8** are attributed to both the redshift of the absorption band and the good balance between the LUMO level of the dye and the energy level of the CB of TiO_2 by the introduction of a thiophene unit to the π-conjugation system of the dye. Finally, DSSCs based on the new-type D-π-A fluorescent dyes **NI3**–**NI8** show a good light-soaking stability comparable to those of the conventional D-π-A dye sensitizers **NI1** and **NI2** under simulated solar light (AM 1.5, 100 mW cm^{-2}). After 10 h of light soaking, there is little change in the J_{sc}, V_{oc}, FF, and η values (see Figure S2 in the Supporting Information for the device stability of DSSCs).

Conclusion

As a new-type of D-π-A dye sensitizers for DSSCs, we have designed and synthesized fluorescent dyes **NI3**–**NI8** with a pyridine ring as electron-withdrawing-injecting anchoring group. The FTIR spectra of **NI3**–**NI8** adsorbed on TiO_2 nanoparticles indicate the formation of strong coordinate bonding between the pyridine ring of the dyes and the Lewis acid sites of the TiO_2 surface. The J_{sc} and η values of DSSCs based on **NI3**–**NI8** are greater than those of the conventional D-π-A dye sensitizers **NI1** and **NI2** with a carboxyl group as electron-withdrawing anchoring group. Consequently, it was demonstrated that the formation of coordinate bonds between the pyridine ring of dyes **NI3**–**NI8** and the Lewis acid sites of the TiO_2 surface leads to efficient electron injection owing to good electron communication between them, rather than the formation of an ester linkage between the dyes **NI1** and **NI2** and the Brønsted acid sites of the TiO_2 surface. Thus, we propose the use of a pyridine ring as not only electron-withdrawing anchoring group but also electron-injecting group in a new-type of D-π-A dye sensitizers for DSSCs. Furthermore, it is expected that D-π-A fluorescent dyes **NI3**–**NI8** are Type-II sensitizers with a direct electron injection mechanism from the ground state of the dye to the CB of TiO_2 because of coordinate bonding between the pyridine ring of dyes **NI3**–**NI8** and the Lewis acid sites of the TiO_2 surface. Further studies to elucidate whether the fluorescent dyes **NI3**–**NI8** are Type-I or Type-II sensitizers are now in progress based on transient absorption spectroscopy and the transient photovoltage techniques.

Experimental Section

General: IR spectra were recorded on a Perkin–Elmer Spectrum One FTIR spectrometer by the attenuated total reflectance (ATR) method. Absorption spectra were observed with a Shimadzu UV-3150 spectrophotometer and fluorescence spectra were measured with a Hitachi F-4500 spectrophotometer. The fluorescence quantum yields in solution and in the solid state were determined by a Hamamatsu C9920-01 instrument equipped with a charge-coupled device (CCD) by using a calibrated integrating sphere system (λ_{ex} = 370 nm). Cyclic voltammetry (CV) curves were recorded in CH_2Cl_2/Bu_4NClO_4 (0.1 M) solution with a three-electrode system consisting of Ag/Ag^+ as reference electrode, a Pt plate as working electrode, and a Pt wire as counter electrode by using a Hokuto Denko HAB-151 potentiostat equipped with a function generator.

Computational methods: Semiempirical calculations were carried out with the WinMOPAC Version 3.9 package (Fujitsu, Chiba, Japan). Geometry calculations in the ground state were made by using the AM1 method. All geometries were completely optimized (keyword PRECISE) by the eigenvector following routine (keyword EF). Experimental absorption spectra of the compounds were compared with their absorption data by the semiempirical method INDO/S (intermediate neglect of differential overlap/spectroscopic). Dipole moments of the compounds were also evaluated from INDO/S calculations. All INDO/S calculations were performed by using single excitation full SCF/CI (self-consistent field/configuration interaction), which included the configuration with one electron excited from any occupied orbital to any unoccupied orbital, for which 225 configurations were considered [keyword CI (15 15)].

Preparation of DSSCs based on dyes NI1–NI6: The TiO_2 paste (JGC Catalysts and Chemicals Ltd., PST-18NR) was deposited on a fluorine-doped tin oxide (FTO) substrate by doctor-blading, and sintered for 50 min at 450 °C. The 9 μm thick TiO_2 electrode (0.5 × 0.5 cm^2 in photoactive area) was immersed in a 0.1 mM dye solution in tetrahydrofuran for a number of hours, enough to adsorb the photosensitizer. DSSCs were fabricated by using the TiO_2 electrode thus prepared, with Pt-coated glass as a counter electrode and a solution of iodine (0.05 M), lithium iodide (0.1 M), and 1,2-dimethyl-3-propylimidazolium iodide (0.6 M) in acetonitrile as electrolyte. The photocurrent–voltage characteristics were measured with a potentiostat under simulated solar light (AM 1.5, 100 mW cm^{-2}). IPCE spectra were measured under monochromatic irradiation with a tungsten–halogen lamp and a monochromator. The amount of adsorbed dye on TiO_2 nanoparticles was determined by absorption spectral measurement of the concentration change of the dye solution before and after adsorption. Absorption spectra of the dyes adsorbed on TiO_2 nanoparticles were recorded on the dye-adsorbed TiO_2 film (thickness of 9 μm) in the diffuse-reflection mode with a calibrated integrating sphere system.

Acknowledgements

This work was supported by Grants-in-Aid for Young Scientists (B) (22750179) from the Japan Society for the Promotion of Science (JSPS) and by the Fujii Research Foundation from Hiroshima University. Y.O. also acknowledges the Nissan Chemical Industries Award in Synthetic Organic Chemistry, Japan.

[1] a) B. O'Regan, M. Grätzel, *Nature* **1991**, *353*, 737; b) A. Hagfeldt, M. Grätzel, *Chem. Rev.* **1995**, *95*, 49; c) U. Bach, D. Lupo, P. Comte, J. E. Moser, F. Weissörtel, J. Salbeck, H. Spreitzer, M. Grätzel, *Nature* **1998**, *395*, 583; d) M. Grätzel, *Nature* **2001**, *414*, 338.
[2] a) N. Robertson, *Angew. Chem.* **2006**, *118*, 2398; *Angew. Chem. Int. Ed.* **2006**, *45*, 2338; b) N. Robertson, *Angew. Chem.* **2008**, *120*, 1028; *Angew. Chem. Int. Ed.* **2008**, *47*, 1012.
[3] Z. Chen, F. Li, C. Huang, *Curr. Org. Chem.* **2007**, *11*, 1241.
[4] P. Xie, F. Guo, *Curr. Org. Chem.* **2007**, *11*, 1272.
[5] Z. Ning, H. Tian, *Chem. Commun.* **2009**, 5483.

[6] Y. Ooyama, Y. Harima, *Eur. J. Org. Chem.* **2009**, *18*, 2903.
[7] A. Mishra, M. K. R. Fischer, P. Bäuerle, *Angew. Chem.* **2009**, *121*, 2510; *Angew. Chem. Int. Ed.* **2009**, *48*, 2474.
[8] A. Hagfeldt, G. Boschloo, L. Sun, L. Kloo, H. Pettersson, *Chem. Rev.* **2010**, *110*, 6595.
[9] H. Choi, I. Raabe, D. Kim, F. Teocoli, C. Kim, K. Song, J.-H. Yum, J. Ko, M. K. Nazeeruddin, M. Grätzel, *Chem. Eur. J.* **2010**, *16*, 1193.
[10] M. K. R. Fischer, S. Wenger, M. Wang, A. Mishra, S. M. Zakeeruddin, M. Grätzel, P. Bäuerle, *Chem. Mater.* **2010**, *22*, 1836.
[11] A. Listorti, B. O'Regan, J. R Durrant, *Chem. Mater.* **2011**, *23*, 2381.
[12] T. Bessho, S. M. Zakeeruddin, C.-Y. Yeh, E. W.-G. Diau, M. Grätzel, *Angew. Chem.* **2010**, *122*, 6796; *Angew. Chem. Int. Ed.* **2010**, *49*, 6646.
[13] S. Paek, H. Choi, C. Kim, N. Cho, S. So, K. Song, M. K. Nazeeruddin, J. Ko, *Chem. Commun.* **2011**, *47*, 2874.
[14] Y. Ooyama, S. Inoue, T. Nagano, K. Kushimoto, J. Ohshita, I. Imae, K. Komaguchi, Y. Harima, *Angew. Chem.* **2011**, *32*, 7567; *Angew. Chem. Int. Ed.* **2011**, 50, 7429.
[15] M. J. S. Dewar, E. G. Zoebisch, E. F. Healy, J. J. Stewart, *J. Am. Chem. Soc.* **1985**, *107*, 3902.
[16] a) J. E. Ridley, M. C. Zerner, *Theor. Chim. Acta* **1973**, *32*, 111; b) J. E. Ridley, M. C. Zerner, *Theor. Chim. Acta* **1976**, *42*, 223; c) A. D. Bacon, M. C. Zerner, *Theor. Chim. Acta* **1979**, *53*, 21; d) H. A. Kurtz, J. J. P. Stewart, D. M. Dieter, *J. Comput. Chem.* **1990**, *11*, 82.
[17] Z.-S. Wang, K. Hara, Y. Don-oh, C. Kasada, A. Shinpo, S. Suga, H. Arakawa, H. Sugihara, *J. Phys. Chem. B* **2005**, *109*, 3907.
[18] a) J. B. Peri in *Catalysis, Science and Technology, Vol. 5* (Eds.: J. R. Anderson, M. Boudart), Springer, Berlin, **1984**, pp. 171–220; b) A. A. Davydov in *Infrared Spectroscopy of Adsorbed Species on the Surface of Transition Metal Oxide* (Ed.: C. H. Rochester), Wiley, Chichester, **1984**; c) M. W. Urban, *Vibrational Spectroscopy of Molecules and Macromolecules on Surfaces*, Wiley, Chichester, **1993**, pp. 171–185.
[19] a) M. I. Zaki, M. A. Hasan, F. A. Al-Sagheer, L. Pasupulety, *Colloids Surf. A* **2001**, *190*, 261; b) V. Vishwanathan, H.-S. Roh, J.-W. Kim, K.-W. Jun, *Catal. Lett.* **2004**, *96*, 23; c) M. M. Mohamed, W. A. Bayoumy, M. Khairy, M. A. Mousa, *Microporous Mesoporous Mater.* **2007**, *103*, 174.

Received: June 22, 2011
Revised: August 4, 2011
Published online: November 22, 2011

